JOURNAL OF GEOPHYSICAL RESEARCH, VOL. 112, A10208, doi:10.1029/2007JA012299, 2007

Click Here for Full Article

Observations of structured optical emissions and particle precipitation equatorward of the traditional auroral oval

T. Pedersen,[1] E. Mishin,[2] and K. Oksavik[3]

Received 25 January 2007; revised 10 May 2007; accepted 5 July 2007; published 12 October 2007.

[1] High-sensitivity all-sky images from south-central Alaska show the common occurrence of slow-moving, faint optical emissions at 557.7 and 427.8 nm well equatorward of the discrete aurora. These emissions appear over a continuum of forms ranging from homogenous longitudinal bands to bands with irregular structure on their poleward edge to widely distributed arrays of vortex-like curls and widely spaced spots on the order of 10 km in diameter. These forms appear to correspond to various stages in the temporal evolution of nearly corotating precipitation regions populated by particles injected from more distant areas of the magnetosphere and may exhibit morphological control by an instability operating on cold plasma near the plasmapause. Although these phenomena are most common in the evening hours and typically persist for hours at a time, one case demonstrates that the features can remain throughout the night on occasion. These faint optical features appear to be colocated with regions of enhanced background counts in DMSP particle measurements and to be associated with the ring current/outer radiation belt region equatorward of subauroral polarization streams (SAPS). The features can occur in conjunction with HF and MF radio frequency absorption, at levels which are often too low to show up on routine absorption instruments such as the riometer. This has practical implications on the operation and interpretation of ionospheric interaction experiments carried out in the subauroral region.

Citation: Pedersen, T., E. Mishin, and K. Oksavik (2007), Observations of structured optical emissions and particle precipitation equatorward of the traditional auroral oval, *J. Geophys. Res.*, *112*, A10208, doi:10.1029/2007JA012299.

1. Introduction

[2] Auroral precipitation has generally been classified into two broad categories: discrete aurora consisting of various distinct arcs, bands, curls, and similar structure, and diffuse aurora, representing regions of relatively homogenous luminosity. Diffuse aurora are thought to be the primary source of auroral emission near the equatorward edge of the auroral oval, especially in the evening sector [*Feldstein and Galperin*, 1985]. Complicating this picture, there have been a number of reports of detached structures equatorward of the main body of either discrete or diffuse auroral precipitation, going back to the ISIS-2 satellite in the late 1970s [*Anger et al.*, 1978]. *Ono et al.* [1987] reported a drifting spot-like structure in the hydrogen aurora equatorward of the main auroral emission. *Mendillo et al.* [1989] observed large (several hundred kilometers in diameter) patches of enhanced 630.0 nm emission equatorward of the diffuse aurora, and even obtained incoherent scatter radar profiles indicating electron density enhancements in the lower ionosphere associated with the features. *Zhang et al.* [2005] recently showed satellite observations of detached precipitation regions equatorward of the main auroral oval down to very low latitudes during large magnetic storms. Their findings suggested that these features result from precipitation of ring current (RC) ions. Numerous satellite observations have shown that intense RC ion precipitation events at subauroral latitudes are embedded within the subauroral polarization stream (SAPS) [e.g., *Foster and Burke*, 2002; *Mishin and Burke*, 2005, and references therein]. In the ionosphere there can also be significant changes in the SAPS flow itself on timescales of a few minutes [e.g., *Erickson et al.*, 2002; *Mishin et al.*, 2002; *Oksavik et al.*, 2006].

[3] On the basis of high-sensitivity optical measurements from central Alaska, *Kubota et al.* [2003] identified a significant body of optical emissions and particle precipitation appearing equatorward of the nominal auroral oval during quiet conditions, which they termed corotating aurora. In a review of the *Kubota et al.* [2003] findings, *Newell* [2003] referred to the high degree of structuring observed by Kubota et al. as "seen only in discrete arcs," implying that there may be some discrete auroral processes at work in the diffuse aurora. We note that *Kubota et al.* [2003] referred to the structure as "patches," a term that has

[1]Space Vehicles Directorate, Air Force Research Laboratory, Hanscom Air Force Base, Massachusetts, USA.
[2]Institute for Scientific Research, Boston College, Chestnut Hill, Massachusetts, USA.
[3]Johns Hopkins University Applied Physics Laboratory, Laurel, Maryland, USA.

Copyright 2007 by the American Geophysical Union.
0148-0227/07/2007JA012299$09.00

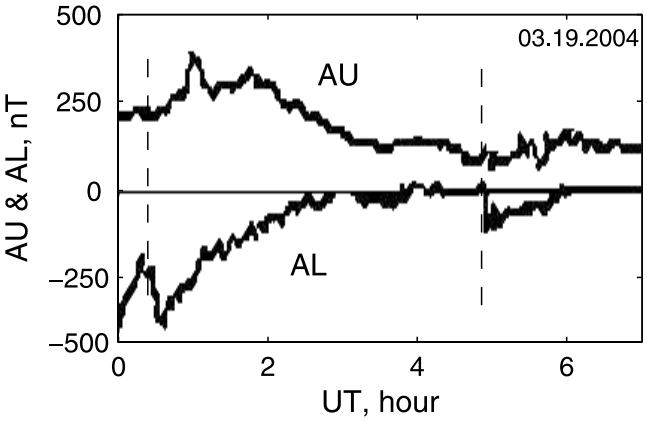

Figure 1. Provisional *AU* and *AL* indices for 19 March 2004 corresponding to the evening sector at HAARP.

a history of usage in reference to diffuse auroral features. Characteristics of the corotating aurora as reported by *Kubota et al.* [2003] and *Toyoshima et al.* [2003] include optical emissions at 557.7 (O^1 S) and 427.8 nm (N_2^+) but not at 630 nm (O^1D) or hydrogen wavelengths, occurrence limited primarily to the magnetic evening local time sector, location within the plasmasphere at least on occasion, particle energies greater than a few keV, absence of ion precipitation, and persistence over periods of hours with only slow motion relative to the earth's surface.

[4] In this paper we report observations of similar optical features equatorward of the traditional auroral oval from a lower-latitude site in south-central Alaska. Observations from this vantage point show this type of precipitation to be present a surprising fraction of the time, to appear in a variety of forms ranging from homogenous bands to small isolated spots, and to be commonly associated with localized absorption of HF and MF radio waves. Coincident observations from the Defense Meteorological Satellite Program (DMSP) and National Oceanic and Atmospheric Administration (NOAA) satellites show the features to be located within regions of elevated radiation belt (RB) particle fluxes well equatorward of the auroral zone, even equatorward of the SAPS region.

[5] Although the occurrence of this phenomenon is most common in the evening MLT sector, we present cases where the features persisted throughout the night, and additionally show observations of sudden onset events and injections creating or renewing the population of precipitating electrons. Our data suggest that an instability operates on the precipitation regions, especially the poleward edge of the more homogenous forms, which also appear to be inclined relative to contours of magnetic latitude. The range of forms observed appears to correspond to different stages in the evolution of the precipitation regions. A particularly common manifestation is widely distributed fields of small localized subvisual swirls spanning regions many degrees of latitude in extent mostly equatorward of the SAPS.

2. Observations

[6] Observations were made at the High Frequency Active Auroral Research Program (HAARP) facility in Gakona, Alaska (62.4 N, 145.2 W, 63.6 N magnetic) during research campaigns carried out since February 2004, when higher-sensitivity all-sky imagers were first employed at the site. Optical data from both ionospheric heating experiments and natural geophysical phenomena were collected with 3.5 and 4 inch 180° field-of-view all-sky imagers, mostly operated in bare CCD mode without image intensifiers. Prior to field deployment, the imagers were calibrated against a low-light current-controlled tungsten lamp calibration source to determine the CCD bias, count rate, and dark count rate in the configuration utilized. Instrument vignetting and Van Rhijn brightening away from zenith offset each other to first order and have not been corrected for in these images, so the calibrated apparent surface brightness is strictly valid only for the image center. As anticipated artificial optical effects were on the order of a few hundred Rayleighs (R) at 630 nm and only tens of R at 557.7 nm, the instruments were optimized for operation at extremely low light levels rather than for typical auroral intensities of many kR. Although the HAARP transmitter operated at some point during each of the periods studied in this paper, we have thus far been unable to detect any perturbation of the natural subauroral precipitation by the transmitter. The precipitation is often present before any transmissions begin, typically extends over a much wider area than could be directly influenced by the transmitter beam, and is unaffected by major changes in transmitter modes including changes in frequency and polarization, on/off cycling, or the end of daily operations, confirming its character as a natural phenomenon. As will be discussed later, however, this type of natural precipitation has significant impacts on HAARP operations, especially due to absorption of the HF waves in the ionospheric D region.

[7] It is worth noting that the geophysical conditions during and before the events studied can be characterized as slightly perturbed. All events were for Kp = 0–2, and they occurred a few hours after Kp was 3–4. For all events the provisional Dst (or SYM-H) index was in the range −30 to −10 nT. Figure 1 shows (provisional) auroral *AU* and *AL* indices on 19 March 2004, obtained through the Web site of the World Data Center for Geomagnetism, Kyoto. One can see two unmatched excursions in the *AL* index at ~0030 and 0450 UT, indicating brief developments of the *DP* 1 system, i.e., the onset of either substorms or pseudobreakups. On 16 February 2004, another date to be discussed, a similar magnetic disturbance occurred at about 0100 UT.

2.1. Movie of Image Data From 19 March 2004

[8] Images acquired over a 5-hour period spanning the evening magnetic local time (MLT) sector on 19 March 2004 provide an excellent example of the range of optical features present in the region equatorward of the traditional auroral oval and also capture the creation and evolution of the precipitation structure in this particular event. The dynamic creation events and subsequent motion and evolution of the small-scale structures can be best appreciated through viewing a time-lapse composite color movie of the all-sky images, included in electronic versions of this article (Animation 1). The composite color movie utilizes calibrated data at 630.0, 557.7, and 427.8 nm wavelengths

[1] Animation 1 is available in the HTML.

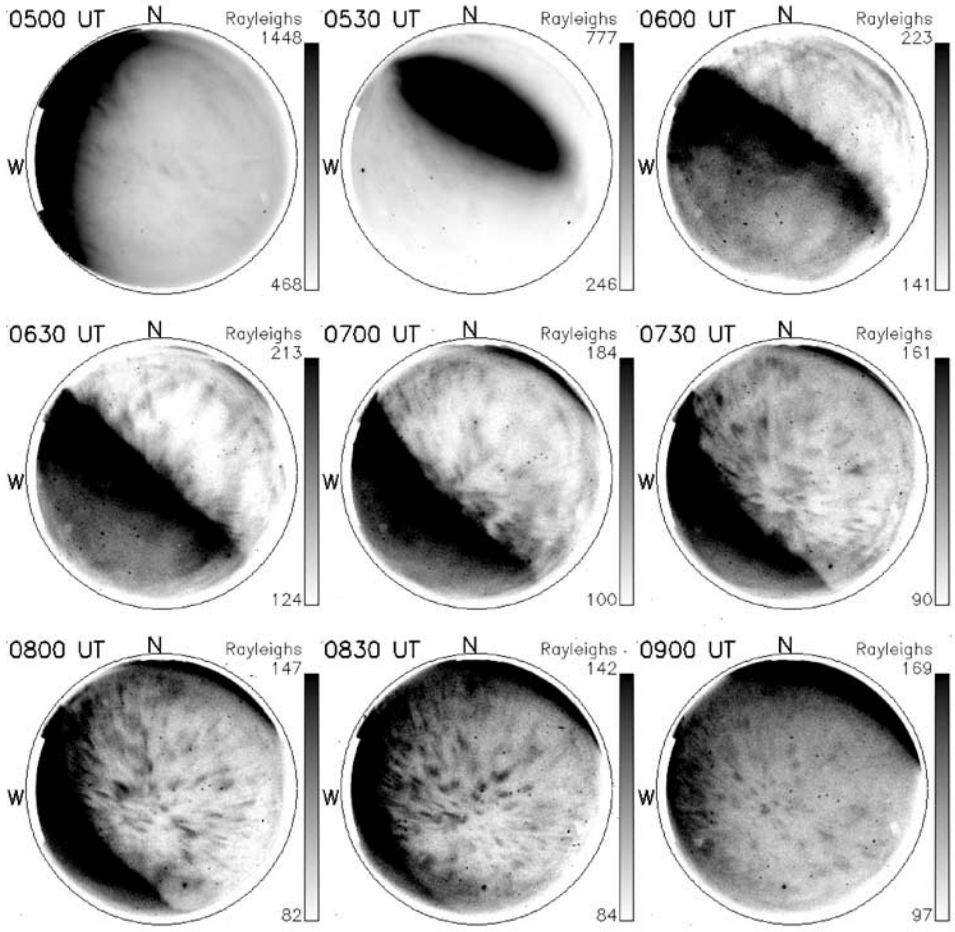

Figure 2. Green-line (557.7 nm) all-sky images shown at half hour intervals for the events on 19 March 2004. Images are shown in negative for enhanced visibility of small-scale structure, with brightest features appearing black.

(O^1D, O^1S, and N_2^+ first negative band) for the red, green, and blue channels, respectively, taken at a rate of one frame per minute for each filter. Each frame in the movie has been scaled in intensity based on the statistical properties of the image. Individual images at 557.7 nm for this period are presented in negative format (where black identifies the brightest features) for reference at 30 min intervals in Figure 2. These images have been contrast-stretched to reveal fainter structure and provided with calibration scales indicating the intensity range for each image.

[9] Prior to the optical observations on this day, the HAARP transmitter performed several pulse experiments for radar diagnostics from 0000 UT to 0400 UT, and was then idle until 0502:30 UT. Acquisition of optical data began at 0500 UT (~1810 MLT) with the last remnants of twilight fading in the west. Soon afterward an arc-like band entered the field of view from the northwest, moving equatorward while growing toward magnetic east. By 0545 UT the original band had spread over the southern half of the field of view to create a region of relatively featureless diffuse emissions ending at a sharp boundary near overhead. Some gravity waves propagating toward the SE appear in the image data at this time but are not relevant to this discussion.

[10] As the boundary of the diffuse region gradually moves equatorward after 0600 UT, it becomes clear that the boundary is not aligned with contours of magnetic latitude (nominal declination 24°E) but is instead inclined approximately 45° from geographic E–W, or about 21 degrees from the magnetic E–W direction. It is also becomes apparent that the less luminous region between the diffuse emissions and the normal aurora barely detectable on the far northeastern horizon is not empty but is actually filled with small swirling structures moving in near unison. The synchronous swirling motion of these wispy structures filling the round all-sky images in this time-lapse movie brings to mind the legendary medieval debate regarding the number of angels that can dance on the head of a pin. Given the frequent appearance of these features in our data and the lack of existing terminology to describe them, this visual impression has led us to refer to these widely distributed small spots and swirling curl-like structures as auroral angels.

[11] The brighter parts of the homogenous region have intensities of ~250 R in the green line at 0600 UT, while the angels are about ~150 R, only 30 or 40 R above the sky background of ~110 R. Over the course of several hours, the angels drift primarily westward, with localized vorticular circulation that appears clockwise in the map coordinates of

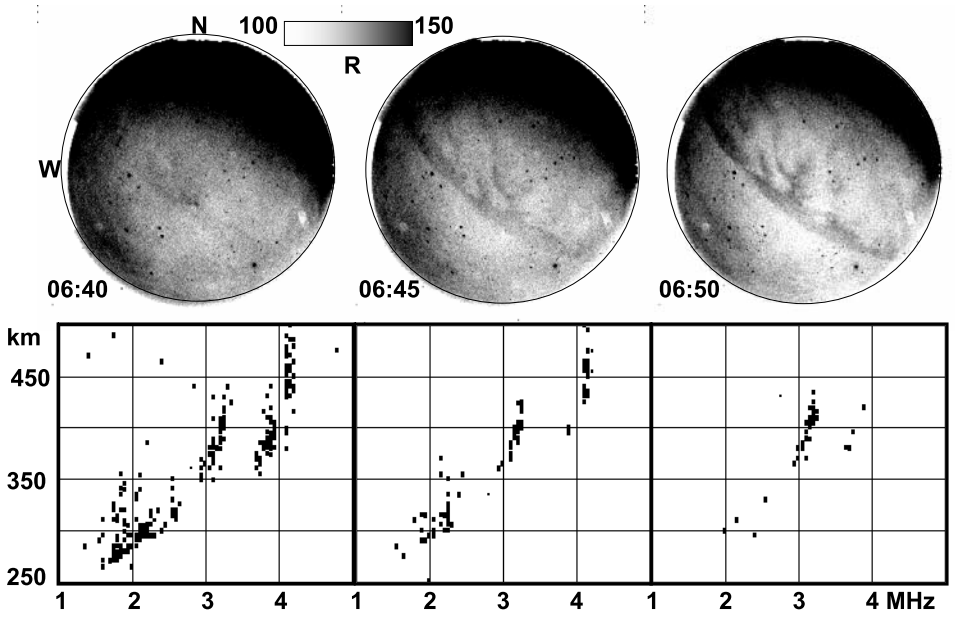

Figure 3. (top) All-sky images at 557.7 nm and (bottom) ionograms at 5 min resolution from 23 March 2004. The all-sky images are shown in negative.

the time-lapse movie, corresponding to counterclockwise (CCW) rotation when viewed antiparallel to the magnetic field. For a short time near 0730, the angels appear to reverse their overall motion and possibly the direction of vorticity before resuming westward motion and CCW rotation. Another phenomenon of note, especially near 0700 UT, is the slightly rippled poleward boundary of the diffuse region that appears to be linked to filaments leading perpendicularly out of the boundary and possibly connecting to the angel structures. At 0830 UT the main body of the homogenous region is near the southern edge of the field of view while the ordinary aurora has appeared on the far northeastern horizon. Geographic mapping of the images at this time indicates that the poleward boundary of the homogenous region is separated from the ordinary aurora by approximately 5° in latitude, with the equatorwardmost precipitation at least 7° from the traditional auroral oval. The individual small-scale structures at this time are about 10 km across, separated from adjacent enhancements by a similar distance. The dispersed angels persist until the ordinary aurora, which is much more closely aligned with contours of magnetic latitude, moves in and washes out the fainter structures after 0930 UT.

[12] Ionospheric echoes from the HAARP ionosonde disappeared at 0525 UT, when the equatorward edge of the bright band approached the overhead position, and remained absent for the duration of the event, indicating the presence of particles with energy sufficient to ionize the D region below 100 km altitude and absorb HF radio waves. A closer inspection of the early twilight frames of the movie, however, shows the presence of numerous angels even before the injection event, indicating that at least the later stages of this lower-latitude precipitation can occur without significant absorption. Note that these earliest frames were taken toward the end of a 1-hour pause in HAARP operations, and the angels present at that time cannot have been affected by any HF from the facility. During the period from 0502:30 to 0659:29 UT the transmitter alternated between 2.5 min on and 2.5 min off, with no observable differences between on and off periods. No detectable changes were seen in the precipitation during a frequency change at 0527:30 UT or a change to X-mode VLF modulation at 0700 UT.

2.2. Sudden Appearance of Precipitation

[13] In most cases in our data set, the subauroral precipitation features are already present in some form when data acquisition begins at twilight, in agreement with the report of *Kubota et al.* [2003]. The event of 19 March 2004 presented in the previous section, however, showed an injection from higher latitudes creating a diffuse auroral feature and numerous angel structures well equatorward of the nominal auroral oval. Several nights later, on 23 March, a band of hard precipitation with irregular structure on its poleward edge was observed to appear in place and gradually evolve into widely dispersed angels similar to the earlier event.

[14] Figure 3 shows all-sky images and ionograms at 5 min intervals from 0640 to 0650 UT on 23 March 2004. This event occurred in the middle of a heating experiment utilizing a 4 min on 1 min off transmitter cycle, but again the precipitation showed no changes between transmitter on and off periods, and was also completely unaffected by a switch to X-polarization transmissions for another experiment at 0700 UT. At 0640 UT the sky is clear, with ordinary aurora far to the northeast creating a brightness gradient in that sector of the images. By 0645 UT a narrow band extending across the field of view from NW to SE has appeared near overhead. This band has a smooth equatorward boundary, but complicated irregular structure on the poleward edge, which becomes even more apparent at 0650 UT. The band is extremely faint, measuring only about 10 R above the background sky brightness. At the scaling required to resolve this faint feature, the washed out

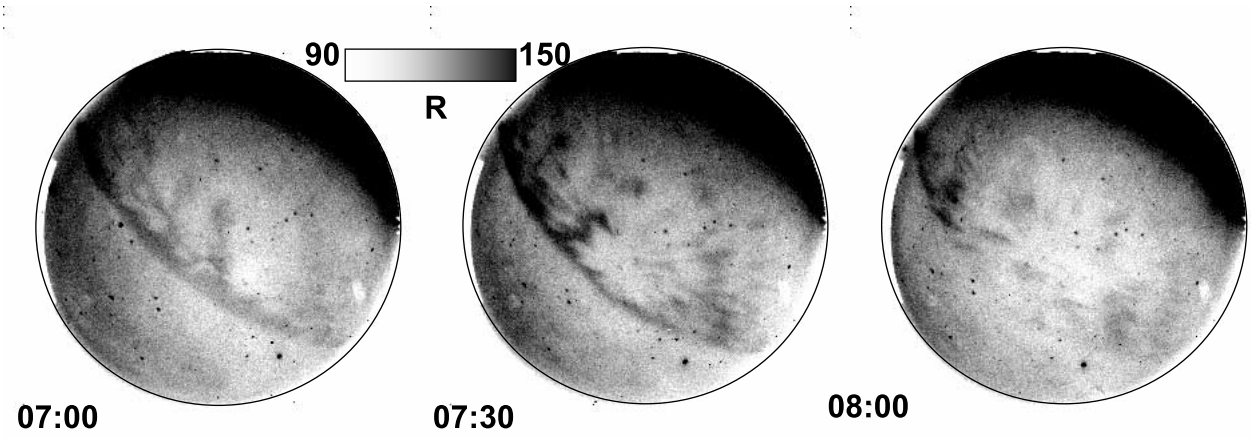

Figure 4. All-sky images at 557.7 nm from 23 March 2004 at half hour intervals. Images are shown in negative.

region of the image toward the ordinary aurora follows a contour of approximately 150 R, or 50 R above the background, and represents scattered light and the high altitude projection of still distant aurora.

[15] The HAARP ionosonde showed the number and strength of ionospheric echoes from the F region dropping rapidly during this 10 min period as the band of hard precipitation appeared, even though the frequency of the vertical asymptotes representing the F region density did not seem to change significantly and no E region traces appeared.

[16] Figure 4 shows the subsequent gradual evolution of this region of hard precipitation over the following hour. The initial band, oriented about 40° to geographic E–W, in contrast with the conventional aurora oriented at about 25° and closely aligned with the magnetic latitude contours (~24°), maintains its smooth equatorward edge while it thins and protuberances grow from the poleward edge. Eventually near 0800 UT the band breaks up into a number of isolated angels drifting slowly off to the west.

2.3. Features Persisting Into Morning Sector, 27 March 2006

[17] On the night of 27 March 2006, structured weak precipitation at 557.7 and 427.8 nm was observed over HAARP almost the entire night. Figure 5 shows images at hourly intervals for this period. On this occasion the all-sky imager was operated with the 180° field of view centered on magnetic zenith and aligned to magnetic rather than geographic coordinates to accommodate other instruments sharing the same mount platform. HAARP operated in a variety of modes during this period, beginning with daytime radar-mode runs at 0000 UT, but shut down for the night at 1200:00 UT. Optical data collection began at 0500 UT but significant twilight in this postequinox data overwhelmed fainter features until almost 0600 UT (~1910 MLT), at which point the sky was mostly filled with small-scale structures about 350 R in intensity, gradually developing into more band-like structures aligned approximately parallel to the local L-shell by 0700 UT. Visual checks of the sky at this time confirmed the subvisual nature of the phenomenon, showing only a clear black sky full of stars. The video-based all-sky camera 325 km to the NNW at Poker Flat, monitored by internet, also showed a clear black sky at this time, the emissions apparently being below its threshold for detection. The band-like structure gradually broke up into a more sparse and irregular distribution by 0800 UT, when some of the brightest regions could just barely be detected by the naked eye. Between 0800 and 0900 UT the features split into a brighter band in the north and a weaker band to the south, with some isolated spots in between. The band gradually broke up over the next three hours, unaffected by the 1200 UT end of HAARP operations, with isolated spots near overhead persisting until approximately 1300 UT (0210 MLT) when they drifted out of the field of view, in this case moving eastward. Data collection ended at 1400 UT (310 MLT) with the approach of morning twilight.

[18] This event was unlike many of the others in that ionosonde echoes were obtained from both F and E regions throughout the night, even when the precipitation was overhead. Significant emissions at 630.0 nm were observed in addition to the standard 557.7 and 427.8 nm signatures, forming a diffuse arc near the equatorward boundary of the small-scale structure. These two facts together indicate that the precipitating particles were significantly lower in characteristic energy than during other events and deposited their energy at higher altitudes where the red line is not quenched and absorption is not generated.

2.4. Absorption-Producing Hard Precipitation on 16 February 2004

[19] A large region of very slow moving 557.7 and 427.8 nm emissions was observed in the evening sector on 16 February 2004. This event began long before any HAARP transmissions were made, progressed unaffected by the nominal HAARP experiment, and persisted well after the end of operations for the night. Ionosonde echoes were found to disappear as the precipitation moved overhead, and did not return for several hours until the precipitation broke up and drifted away as the normal aurora advanced into the

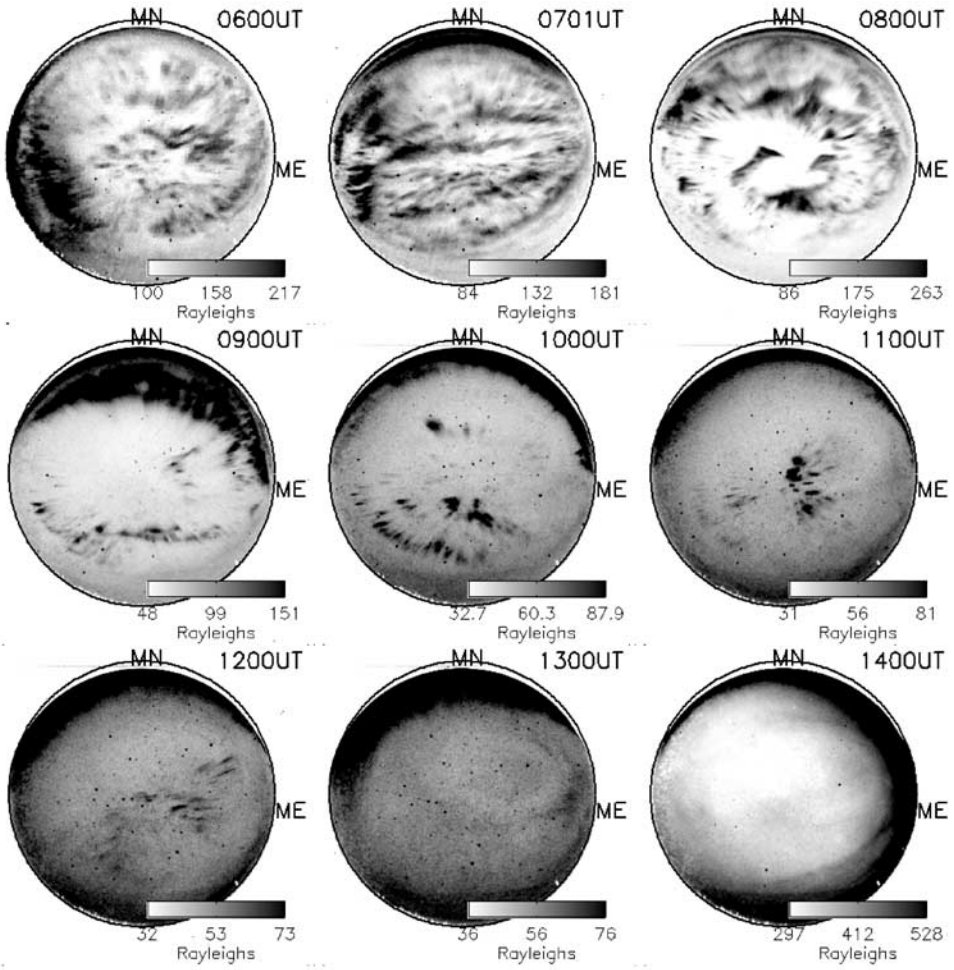

Figure 5. All-sky images at 557.7 nm at hourly intervals for the night of 27 March 2006 (UT). Images are shown in negative and are centered on the magnetic zenith.

field of view. Figure 6 shows the development, at 1 hour intervals, of this event.

[20] The slow moving precipitation region was present when data acquisition began at 0347 UT (~1700 MLT), and had an intensity of about 350 R. No HAARP transmissions were made this evening until 0508:42 UT when the system was tuned up at low power prior to the commencement of an experiment at 0510:00 UT which consisted of alternating 2.5 min periods of full transmitter power and no power. By 0500 UT a large area devoid of emission was noticeable in the east, splitting the emissions into two bands as the features moved slowly toward the overhead position. Ionogram echoes disappeared at about this time. Note that the equatorward edge of the emissions was inclined rather sharply in magnetic latitude: ~45° from geographic N–S at 0500 UT, or ~21° compared to the local magnetic declination of ~24°E, which is again followed closely by the boundary of the ordinary aurora when it appears in the image for 0900 UT. Just after 0600 UT, the thinning band poleward of the emission void flashed several times, after which the interior emission void joined with the poleward void and moved equatorward, leaving behind an irregular distribution of small-scale structure. The entire emission region expanded more rapidly equatorward at this time and began to break up into the now-familiar angels and moved off to the west, a process completed around 0830 UT, when ionogram echoes also returned. The Kodiak SuperDarn radar probing the ionosphere over HAARP from the side showed very low ionospheric velocities (≪100 m/s) but very strong backscatter power (>30 dB) across much of the optical field of view at 0700 UT, indicating the presence of numerous F region irregularities with scale sizes on the order of 10 m. The small spots of optical emission are less apparent in this particular data set because the system at this time was run in an intensified mode resulting in poorer signal-to-noise ratios. Intensities in the remaining precipitation had dropped to about 150 R by 0800 and were no longer detectable by 0900 UT. The HAARP transmitter was shut down for the night at 0719:30 UT at the conclusion of the 2.5 min on/off experiment without any detectable effect on the slowly evolving natural precipitation.

2.5. Satellite Observations on 19 March 2004

[21] A number of satellites passed through or near the imager field of view during the events of 19 March 2004. Figure 7 shows all-sky 557.7-nm green-line images for 0511 and 0645 UT mapped to geographic coordinates at an assumed emission altitude of 110 km and with contours

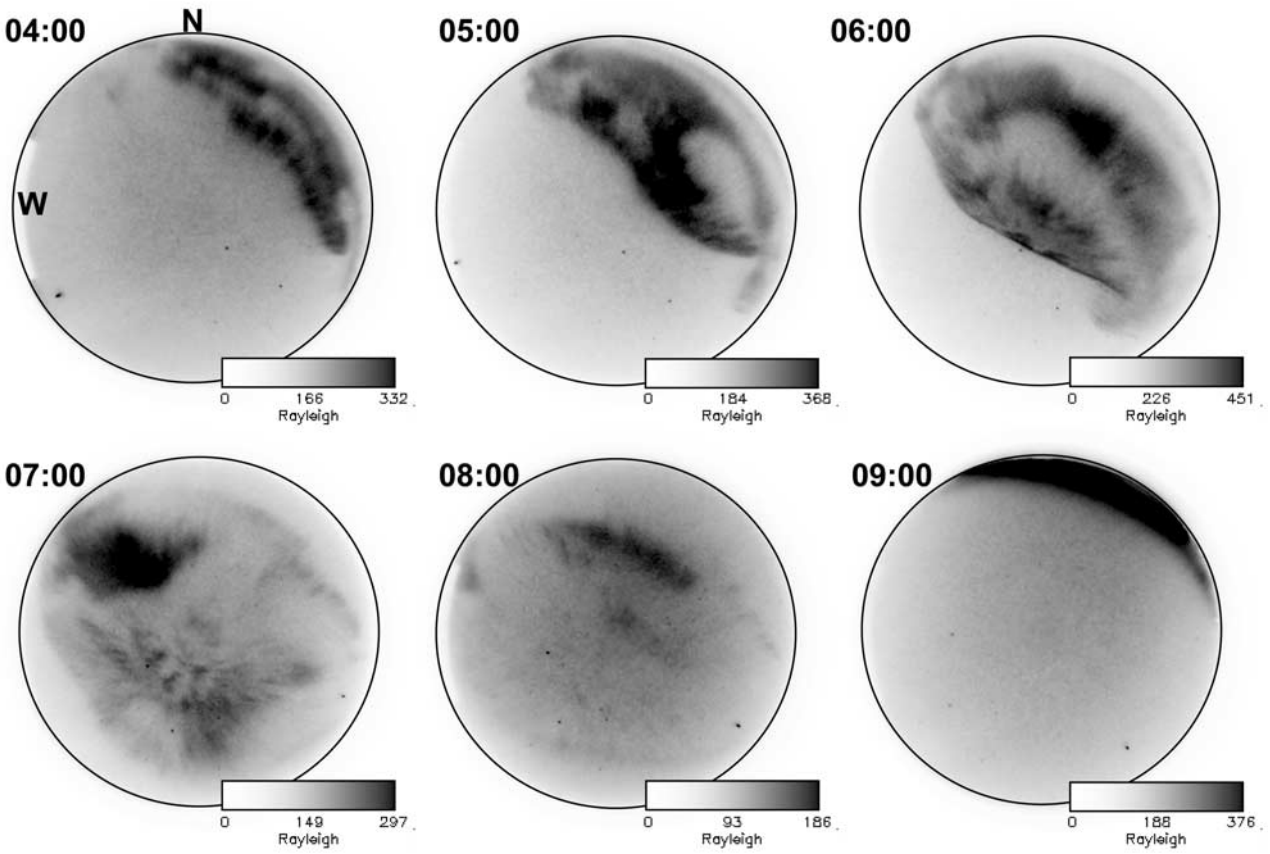

Figure 6. All-sky images at 557.7 nm for the evening of 16 February 2004 (UT). Images are shown in negative.

of magnetic latitude and the tracks of the NOAA 17 and DMSP F15 and F16 satellites superimposed. The arc entering the field of view from the northwest, seen in the movie and in Figure 2, appears just above 65° MLAT in the image for 0511 UT.

[22] DMSP F15 passed just to the NE of the field of view with a closest approach at 0508 UT and was followed by F16 cutting through the twilight at the western edge of the field of view near 0516 UT. The DMSP satellites fly in circular (~840 km altitude), sun-synchronous polar orbits.

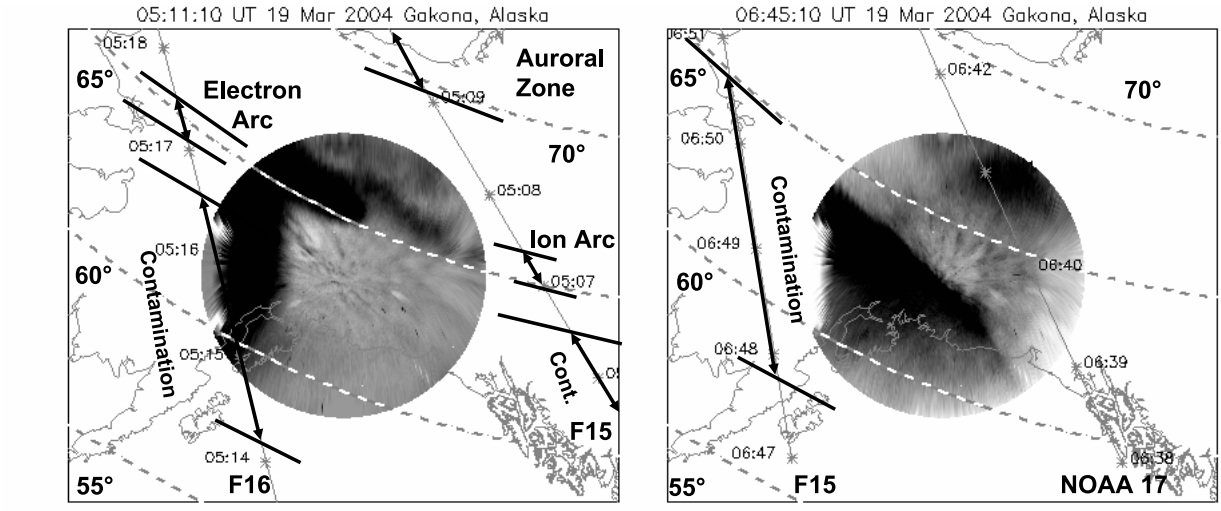

Figure 7. Background-subtracted negative all-sky images at 557.7 nm mapped to geographic coordinates assuming an emission altitude of 110 km and superimposed with the field-line-mapped ground tracks for various satellite passes.

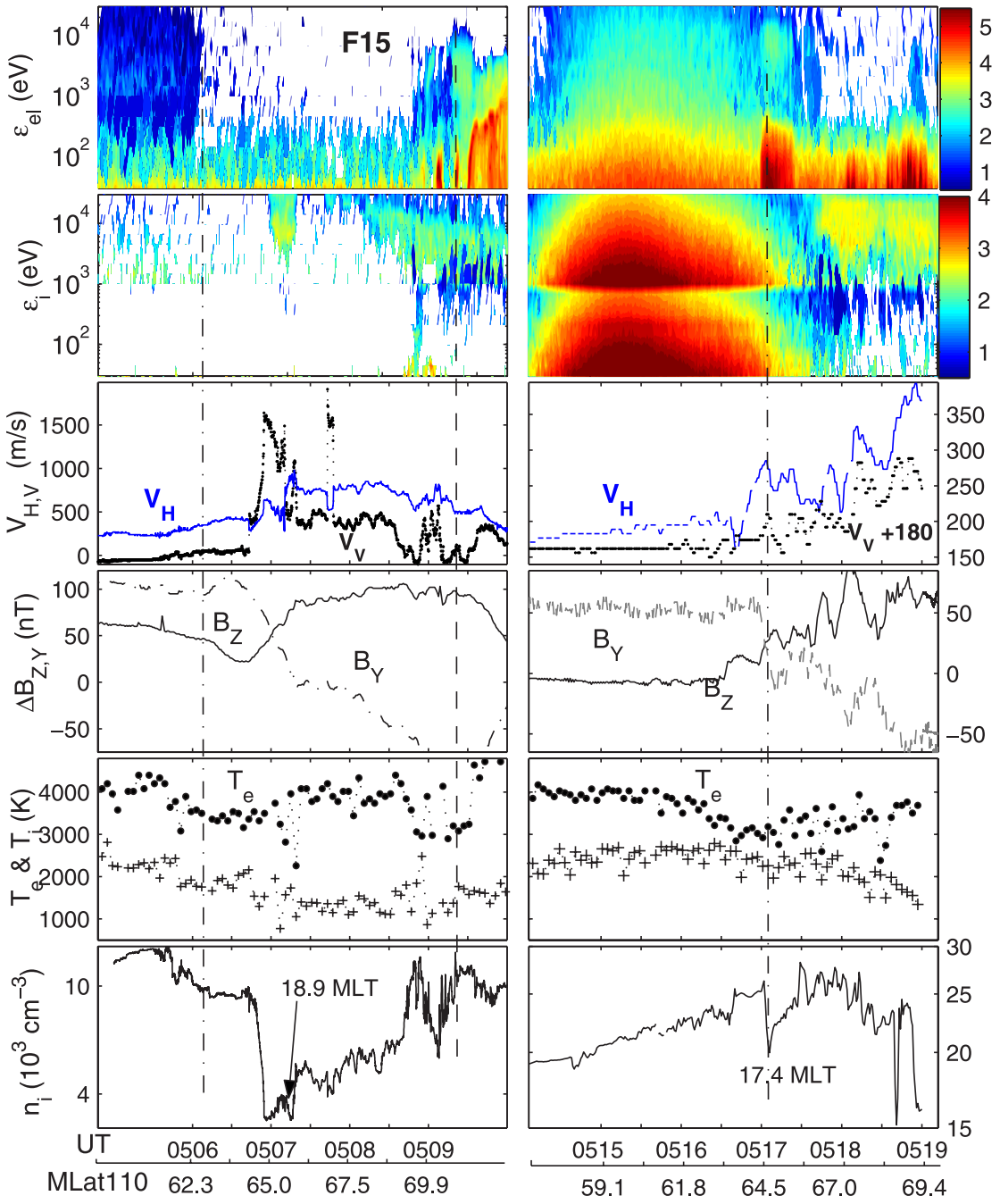

Figure 8. (left) F15 and (right) F16 measurements for overflights near 0511 UT on 19 March 2004. The panels represent electron and ion energy-time spectrograms of downcoming directional differential number fluxes in $cm^{-2} \cdot s^{-1} \cdot ster^{-1} \cdot eV^{-1}$ (logarithmic scale), cross-track drift, in situ magnetic field deviations ΔB_Y and ΔB_Z, ion and electron temperatures, and topside electron densities. Vertical dashed and dash-dotted lines indicate the plasma sheet and the radiation belt precipitation boundaries, respectively.

Each satellite carries a suite of sensors to measure (1) fluxes of precipitating electrons and ions in the energy range 0.03–30 keV (SSJ/4 and, beginning with F16, SSJ/5) [*Hardy et al.*, 1984], (2) the densities, temperatures and drift motions of ionospheric ions and electrons (SSIES) [*Rich and Hairston*, 1994], and (3) perturbations of the geomagnetic field. Nineteen-point ion and electron spectra are returned once per second. The plasma drift and density measurements are sampled at the rates of 6 and 24 Hz, respectively. Magnetic data used here are 1-s averaged differences $\Delta\mathbf{B} = \mathbf{B} - \mathbf{B}_0$ (the IGRF-90 model) in a satellite-centered coordinate system: **X**-downward, **Y**- along the spacecraft velocity, and the **Z** axis completes a right-hand coordinate system. Positive B_Z components generally point in the antisunward direction. The in-track (Y) component of the electric field is given by $E_Y[\frac{V}{m}] = 10^{-6} V_H[\frac{km}{s}] \cdot B_{0X}[nT]$.

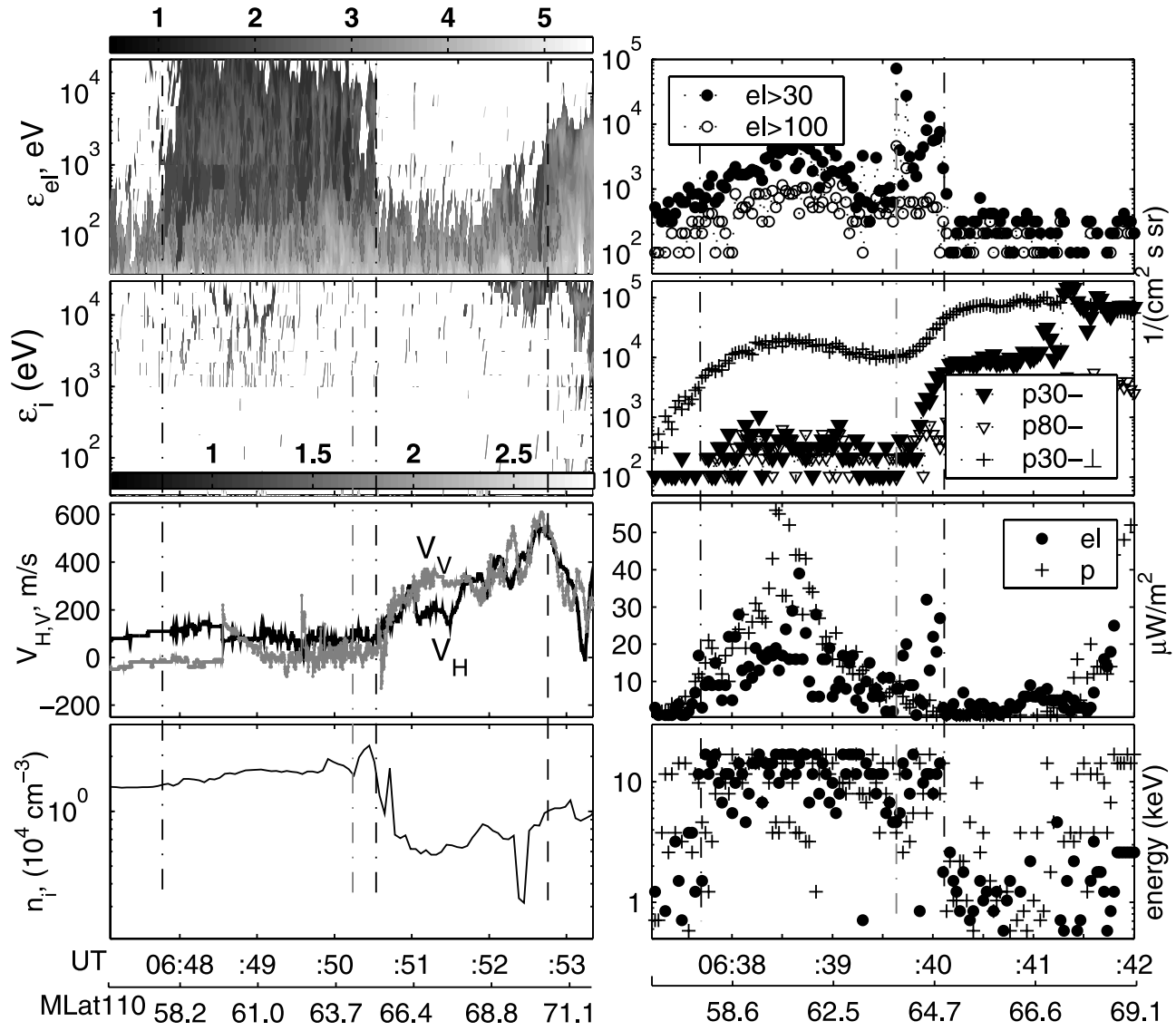

Figure 9. Data from the (left) DMSP F15 satellite and (right) NOAA17 satellite which passed near the field of view near 0645 UT on 19 March 2004. The left hand column shows energy-time spectrograms of directional differential number fluxes of electrons (top frame) and ions (second) in $(\mathrm{cm}^2 \cdot \mathrm{s} \cdot \mathrm{ster} \cdot \mathrm{eV})^{-1}$; the vertical V_V and horizontal V_H components of the cross-track drift velocity in m/s (third); the plasma density (bottom). The right hand column shows directional number fluxes in $(\mathrm{cm}^2 \cdot \mathrm{s} \cdot \mathrm{ster})^{-1}$ of precipitating electrons (top) and precipitating and trapped (⊥) ions (second); the energy flux in the range 0.1–20 keV of electrons (dots) and ions (plus symbols) in μW/m^2 (third); the center energy of the detector band in the range 0.1–20 keV with the highest number of counts (bottom). The vertical dashed and dash-dotted lines indicates the plasma sheet inner boundary and the radiation belt precipitation, respectively.

[23] Figure 8 shows data from the DMSP F15 (left column) and F16 (right column) passes near 0511 UT. Note the zone of slightly higher electron counts in the particle channels onboard F15 and F16 during 0504:30–0506:10 and 0515:00–0517:10 UT, respectively. These are generally interpreted as spurious counts from MeV RB particles penetrating the instrument and striking the detectors directly and are often removed from the data as background contamination (F. Rich, personal communication, 2006). Data from the DMSP F15 satellite shows a number of typical substorm-related subauroral features. First, the shape of the ion traces adjacent to the boundary of the conventional auroral zone, encountered by the satellite at 70° MLat, is characteristic of substorm RC injection events and consistent with the 0450 UT onset [cf. *Mishin and Burke*, 2005]. Second, a broad-spectrum ($2 \leq \varepsilon_i \leq 30$ keV) ion arc near 0507 UT is colocated with large vertical ion flow of more than 1 km/s, an irregular density trough, and ΔB_{YZ} variations. Overall, the F15 data are indicative of a weak, $E_Y \simeq 35\ \frac{\mathrm{mV}}{\mathrm{m}}$, subauroral polarization stream (SAPS) [e.g., *Foster and Burke*, 2002] in the slot region near dusk. The first SAPS/trough patterns after the earlier substorm onset

were detected from previous dusk sector satellite passes at ~0052 and 0140 UT near −61.5° MLat (21.4 MLT) and 62° MLat (20.6 MLT), respectively.

[24] The SAPS-related magnetic variation indicates that the satellite encountered a sheet-like structure of field-aligned currents (FACs) at an attack angle $\alpha \simeq 50°$. This implies an approximately L-shell-aligned current sheet. Positive slopes in the ΔB_Z trace correspond to FACs into ($j_\parallel^\downarrow$) the ionosphere. For a satellite traveling poleward at a speed of 7.5 km/s, one has $j_\parallel^\downarrow[\frac{\mu A}{m^2}] = \frac{1}{\mu_0}\frac{\partial \Delta B_Z}{\partial Y \cos\alpha} \approx 0.15\frac{\partial}{\partial t}\Delta B_Z[\mathrm{nT}] \simeq 0.3\,\frac{\mu A}{m^2}$, which is typical of the SAPS (μ_0 is the permeability of free space). The Poynting flux during this period is evaluated as $S_X^\downarrow \simeq 0.8 E_Y[\frac{V}{m}] \cdot \Delta B_Z[\mathrm{nT}] \simeq 1\,\frac{mW}{m^2}$.

[25] The DMSP F16 satellite skimmed through the western edge of the field of view 10 minutes after the F15 pass and also encountered the auroral zone near 70° MLat. This satellite's instruments experienced significant contamination from RB particles between 0514 and 0517:10 UT, but still revealed a localized region of electron precipitation with both a high-energy peak at 5–10 keV and significant fluxes below 300 eV near 65° MLat, just as it would have crossed the arc seen in the northwest quadrant of the image in Figure 7. The electron precipitation was colocated with enhanced and structured horizontal and vertical ion flows, $\Delta B_{Y,Z}$ perturbations, and the plasma density bite-out. Slightly poleward of the electron arc, one can see in the slot region the high-energy (RC) ion traces as in the F15 ion spectrogram, except for the broad-band ion arc, which is absent.

[26] Figure 9 shows two additional satellite passes near 0645 UT, with DMSP F15 crossing ~500 km west of the image center at 0649 UT and the NOAA 17 satellite passing through the eastern part of the field of view near 0640 UT (refer to Figure 7 for the ground tracks). Particle data from F15 show the entire region to be well equatorward of the auroral zone, again encountered near 70° MLat. Similar to the previous orbit, one can see in the slot region weak traces of the ≤30-keV ions at ≥0652 UT, weak SAPS structure, and a now-smooth density trough. This is consistent with the SAPS evolution during the substorm recovery phase [cf. *Mishin and Burke*, 2005]. Slightly enhanced electron counts below ~500 eV near 0650 UT (63.7° MLat) appear to coincide closely with the relatively redder poleward edge of the diffuse region if it extended in the same direction outside the optical field of view to the satellite track. Note that the plasma temperatures do not show any substantial difference between all the DMSP passes. It is also worthy of note that weak westward flows $V_H \sim 100–200$ m/s are observed in the region of elevated electron background well equatorward of the SAPS region, indicating the presence of the so-called penetration electric field [e.g., *Huang et al.*, 2006].

[27] Particle data from NOAA 17 are presented in the right-hand column. For a description of the NOAA spacecraft and energetic particle instruments, see *Evans and Greer* [2000]. The top frame shows directional number fluxes of precipitating electrons in the >30- and >100-keV channels. Precipitating and trapped (⊥) ion number fluxes in the 30–80- and 80–250-keV channels are shown in the second frame. Shown next are the electron (dots) and ion (plus symbol) energy fluxes in the range 0.1–20 keV and the center energy of the detector band with the highest number of counts (bottom). One can see clear boundaries near 0638 and 0640 UT. The population of precipitating particles in the center of the RB region is dominated by ~10-keV electrons and 3–10-keV protons, while the slot/SAPS region is dominated by ≤1-keV electrons and ≥30-keV protons. The contribution from >30-keV electrons becomes substantial near the radiation belt's poleward boundary, beginning simultaneously with the increase in the 30–80-keV precipitating and trapped (⊥) proton fluxes. The flux of trapped protons exceeded the precipitating flux by a factor of ~10 until ~0641:20 UT when the precipitating flux abruptly increased to the same level as the trapped. This transition occurs in the latitude region where the ~30-keV ion traces of about the same magnitude are seen from F15.

[28] These radiation belt boundaries, projected along L-shells to the magnetic west, would coincide with the corresponding boundaries of the region of enhanced background electron counts on the SSJ/4 sensors. This is yet another confirmation of their radiation belt origin. On the other hand, the above NOAA 17 data strongly suggest that some of the SSJ/4 "background" counts are actual measurements of weak ~10- ≥ 30-keV electron precipitation. This conjecture is also supported by the disappearance of ionosonde echoes most likely due to D region absorption caused by >10-keV electron precipitation. It is also worth noting that quite similar particle features are seen in a NOAA satellite pass from the 16 February event.

3. Discussion

3.1. Geophysical Context of Structured Subauroral Precipitation

[29] The characteristics of the optical and precipitation features presented here, namely presence at 557.7 and 427.8 nm but not 630.0 nm, slow motion relative to the Earth's surface, and preferential occurrence in the MLT evening hours during quiet periods, make it clear that the phenomena seen at HAARP are manifestations of "corotating aurora" identified by *Kubota et al.* [2003]. In our case the view is from a few degrees lower magnetic latitude and farther from the nominal auroral oval, although in the same longitude sector. Our optical observations, combined with satellite measurements, show that corotating auroral forms can be present up to 10° equatorward of the traditional auroral oval.

[30] As suggested by *Newell* [2003], *Kubota et al.* [2003], and our own results, there is a strong similarity between corotating auroral regions and the detached arcs first identified in the ISIS-2 data [*Anger et al.*, 1978]. In particular, both our data and that of *Kubota et al.* [2003] are from the Alaskan sector, near the peak occurrence longitude for detached arcs [*Moshupi et al.*, 1979]. We also find that in cases where large-scale boundaries are identifiable in the corotating precipitation, the boundary tends to be inclined more steeply than the local magnetic declination, as would be required for detached arcs connected to the auroral oval farther to the west. The common appearance in our data of the small-scale curl-like features and spots we have referred to as "angels" is also consistent with the early reports of detached arcs described by *Anger et al.* [1978] and *Moshupi*

et al. [1979] to be "frequently very irregular and mottled in appearance."

[31] Our observations are consistent with *Moshupi et al.*'s [1979] suggestion that subauroral forms are regions where precipitation is induced within broader regions of trapped (RB) particles. The RB's inner edge has been demonstrated to be closely related to the innermost plasmapause location [*Goldstein et al.*, 2005a; *Li et al.*, 2006]. In turn, the latter is closely related to the separatrix between open and closed equipotentials defined by the force balance between the dawn-dusk (convection) electric field E_C and the corotation field E_R [e.g., *Chen and Wolf*, 1972]. Simply put, plasma in the region outward of the separatrix drifts sunward to the dayside magnetopause where it is lost, while plasma on closed trajectories can build up. The time delay between plasmapause motions and the IMF polarity transitions is around 20–30 min [e.g., *Goldstein et al.*, 2003], consistent with the relation of E_C to the southward IMF [e.g., *Akasofu*, 1977].

[32] Significantly, most of our observations and earlier reports pertain to the duskside. *Toyoshima et al.* [2003] pointed out a case where corotating aurora at slightly higher latitudes was found to correlate with a plasmaspheric plume (or bulge or tail), i.e., dense plasmaspheric-like plasma outward of the quiet-time plasmapause [e.g., *Moldwin et al.*, 2004, and references therein]. It is understood in terms of the motion of the separatrix due to an imbalance between E_R and time-varying E_C. During the growth phase of a substorm E_C increases, shifting the separatrix inward. Thus plasma at and near the (old) separatrix is in the region of open equipotentials and would rotate sunward. During the recovery phase of an isolated substorm E_C decreases. Accordingly, the separatrix moves outward and the plasma is again trapped and corotates. Since the plasmaspause location L_{pp} depends on MLT and the plasmaspheric density depends on L, the resulting density distribution tends to from a bulge near dusk [e.g., *Chen and Wolf*, 1972].

[33] It has also been established that on average the plasmapause is colocated with the midlatitude trough [*Yizengaw et al.*, 2005; *Yizengaw and Moldwin*, 2005]. In addition to that, the SAPS electric field strips away plasmaspheric plasma in the overlap region, thereby defining either a new plasmapause or plasmaspheric trough [e.g., *Ober et al.*, 1997; *Goldstein et al.*, 2005b]. These features agree with the RB boundary seen just equatorward of the SAPS and trough in Figures 8 and 9. According to the above ("simple") scheme, the bulge/tail should corotate during the recovery phase. However, the angels are observed to drift primarily westward in the dusk sector, consistent with weak sunward convection flows equatorward of the SAPS region in Figures 8 and 9. This indicates the importance of the penetration electric field in the dynamics of the RB region.

3.2. Structuring

[34] The general appearance and localized vorticular circulation of the angel structures suggests they might represent imperfect curls or partial spirals in unresolved or discontinuous filaments of enhanced precipitation. If this inference proves true, this structure would be in common with more typical "discrete" forms of aurora, which often consist of thin arcs modulated by curl and spiral forms. One major difference, besides the characteristic particle energy and many orders of magnitude in emission intensity, would be that in these weak subauroral features there is only minimal preference for alignment along L-shells. In fact, many of the features on the poleward edges of bands appear to be aligned more in the magnetic N–S direction than E–W. The isolated spots often seen in the later stages could be interpreted as curls in filaments that are no longer above the threshold for detection, which would appear as isolated rays when viewed away from the magnetic zenith, although the true small-scale structure cannot be directly determined from these low-resolution all-sky images.

[35] *Moshupi et al.* [1979] and *Wallis et al.* [1979] have concluded that the observed structuring in detached arcs represents spatial modulation of the mechanism producing the precipitation rather than in the distribution of the particles themselves, which is expected to be much more homogenous. *Wallis et al.* [1979] further hypothesized that dense cold plasma in or detached from the dusk side plasmasphere could be responsible for pitch angle scattering, in which case structure observed in the precipitation would reflect structure in the cold plasma.

[36] From the NOAA 17 satellite data it follows that the main contribution to the angels-related precipitation comes from ~10- $\geq$ 30-keV electrons. They likely originate from previous substorm injections and were then trapped inside the plasmasphere subsequent to the separatrix motion under the action of time-varying E_C. Indeed, the substorm expansion onset results in particle injection followed by a recovery period [e.g., *Akasofu*, 1977]. When E_C decreases, the separatrix moves outward. As a result, substorm-injected electrons penetrate into the previously forbidden plasmasphere and, after being trapped, gradient-drift clockwise [*Burke et al.*, 1995; *Liemohn et al.*, 1998]. Their precipitation is due mainly to interaction with whistler mode waves (plasmaspheric hiss). The minimum particle energy required for cyclotron interaction with hiss is defined as

$$\varepsilon_{\min} \simeq \frac{B_L^2}{8\pi n_L} A_0^{-1} \tag{1}$$

[37] Here $A_0 \simeq \langle \varepsilon_\perp \rangle / \langle \varepsilon_\parallel \rangle - 1$ is the 'temperature' anisotropy of energetic electrons (normally <1), $\langle \varepsilon_{\perp/\parallel} \rangle$ (in eV) stands for the average energy perpendicular/parallel to the magnetic field; the values of the plasmaspheric density n_L and magnetic field B_L refer to the equatorial plane. Assuming $A_0 = 0.1$, $n_L = 300$ cm^{-3} and $B_L = 400$ nT ($L \simeq 4$ or MLat $\simeq 60°$), one obtains $\varepsilon_{\min} \simeq 10$ keV. Given a monotonically decreasing distribution against the increasing ε, the number of the resonance particles increases with n_L. In addition, it is well known that a field-aligned density enhancement (duct) is a wave guide for hiss so that waves can interact with electrons along the whole magnetic tube. Given both these effects near the instability threshold, even a small density enhancement should significantly enhance precipitating fluxes. Thus structuring in the plasmasphere might accordingly modulate the precipitation pattern leading to spatially localized optical structures.

[38] Given mapping factors of order 5–10 across the RB region, field-aligned plasmaspheric irregularities of $\lambda_{\perp_p} \sim$ 10–100 km would correspond to ~1–20 km "angels." One means of investigating this is to consider structure in the

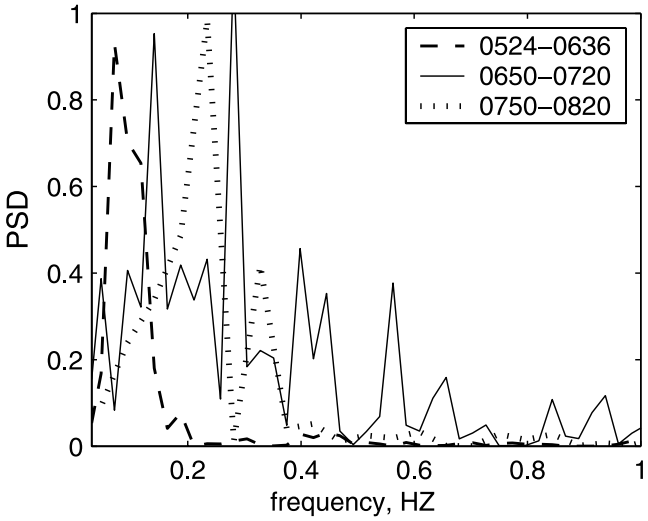

Figure 10. Power spectral density of topside ionospheric irregularities measured by the DMSP F15 satellite. Time intervals in mmss after 0500 UT are indicated.

topside ionospheric density. Figure 8 (bottom) shows significant structures near the RB poleward edge and inside the trough from the DMSP F15 and F16 passes. Figure 10 shows power spectral densities of irregularities along three consecutive parts of the F15 pass. Assuming that the satellite crossed spatially varying structures, one obtains their wavelengths as $\lambda_{\perp i}$[km] $\sim$ 7.5/f, where f is the apparent frequency in Hz. The shortest irregularities ($\lambda_{\perp i} \sim 15-30$ km) are observed within the SAPS region [cf. *Mishin and Burke*, 2005], while near the edge of the angels region the characteristic scale-length is of $\lambda_{\perp i} \sim$ 75 km. This is in a qualitative agreement with the F16 observations. No substantial irregularities are seen within the RB region during the F15 westward pass (Figure 9), while the angels are still present. Thus we conclude that any presumed small-scale plasmaspheric irregularities do not extend to the topside ionosphere.

[39] The widespread presence of auroral angels and the often highly structured poleward edges of corotating auroral forms suggests that their generation process operates across the whole region, being intensified near the plasmapause. There is a large body of experimental evidence in existence of small-scale irregularities inside the plasmasphere and near the plasmapause during, or in the aftermath of, periods of enhanced magnetic activity (for a review, see *Carpenter et al.* [2002] and references therein). Suggested generation mechanisms, like interchange instabilities [e.g., *Pierrard and Lemaire*, 2004], operate near the plasmapause and do not explain how irregularities could appear inside the plasmasphere. However, during transient periods, especially when the inhomogeneous penetration electric field is present well inside the plasmasphere, one anticipates shear plasma flows (differential drift) rather than the exospheric distribution [e.g., *Brice*, 2001]. Shear-driven instabilities are known to be quite an effective source of density irregularities [e.g., *Kadomtsev*, 1965]. Their discussion is well beyond the scope of this observation-based study. It is worthy of note that *Lin et al.* [2007] reported on the observations of strong shear flows near the plasmaspheric plume's boundaries. There is also a recent paper by *Greenwald et al.* [2006] reporting a type of small-scale ionospheric irregularities that are frequently seen in the nightside subauroral ionosphere under similar low-to-moderate Kp conditions with a new over-the-horizon HF radar at Wallops Island, Virginia. They found these small-scale irregularities, similar to those seen over HAARP on 16 February 2004, to be consistent with the temperature gradient instability near the plasmapause described by *Hudson and Kelley* [1976].

3.3. Implications for Ionospheric Heating and HAARP Operations

[40] There are three major HF ionospheric heating facilities in the subauroral or auroral region: HAARP (Gakona, Alaska), HIPAS (Fairbanks, Alaska), and HEATING (Tromso, Norway). Depending on ionospheric conditions and the desired effect, these transmitters can deposit energy in the ionospheric D, E, or F regions at altitudes of about 90, 100, and 250 km respectively. Precipitation of high-energy particles from the magnetosphere has a pronounced effect on these operations, as it enhances the D region which can then absorb the HF radio waves before they can reach higher altitudes.

[41] At HAARP, D-region absorption is a commonly experienced phenomenon, and its presence generally frustrates any E or F region heating experiments. Absorption is typically measured by riometers at frequencies near 30 MHz by comparing instantaneous RF strength from cosmic noise sources with a baseline curve measured or modeled for quiet conditions. The strength of absorption (in dB) generally scales inversely with the frequency squared [cf. *Rosenberg et al.*, 1991]. At HAARP during nighttime experiments at solar minimum, where the maximum ionospheric plasma frequency is typically 3 MHz or less, this strong frequency dependence means that transmitted waves can suffer severe attenuation without significant absorption registering on a traditional riometer.

[42] Ionospheric heating has been conducted at HAARP since 1999, and many aspects of the heating, especially in artificial optical emission experiments, have been difficult to reproduce, with identical transmitter modes often generating an order of magnitude difference in output between runs, even under nominally similar ionospheric conditions. The common occurrence of subauroral particle precipitation at HAARP capable of creating HF absorption well below the sensitivity threshold of riometers at 30 MHz, only recognized recently because of improved optical diagnostics, now offers a potential explanation for much of this variability. Given the highly structured nature of corotating auroral precipitation, spatial structure seen in optical emissions produced by heating experiments may also reflect absorption "shadowing" of the beam rather than actual structure in the higher levels of the ionosphere, whether natural or created by the transmitter. An example of this effect, where artificial 630 nm red line emissions fill in the gaps between natural precipitation structures prominent in the 557.7 nm green line is shown in the work of T. R. Pedersen et al. (Observations of artificial and natural optical emissions at the HAARP facility, accepted by *Annales Geophysicae*, 2007). Researchers should be aware that the nominally benign subauroral conditions often encountered

at HAARP are often actually a center of extreme structuring in near-Earth space.

[43] Another application of ionospheric heating research at these latitudes is artificially induced particle precipitation through cyclotron resonance with VLF waves generated by modulation of the ionospheric D-region current [e.g., *Stubbe et al.*, 1981; *Inan et al.*, 2004]. The required conditions for inducing artificial precipitation using an HF heater are (1) significant D layer ionization to absorb the transmitter power in current-carrying layers, (2) significant currents that can be modulated to create VLF waves, (3) ducts to carry the waves deep into the magnetosphere, and (4) a population of trapped particles that can be scattered into the loss cone. A comparison of these requirements with the conditions associated with structured subauroral precipitation shows that these conditions are likely to be an ideal testing ground for attempts to induce particle precipitation. Additionally, SAPS-related current systems may provide significant electric fields and currents, at least in certain phases of activity.

4. Conclusions

[44] We have presented high-sensitivity optical observations of faint subauroral precipitation taking the form of diffuse and highly structured green line emissions on the order of 100 R in intensity located up to 10° equatorward of the traditional auroral oval. These optical structures appear to be associated with highly energetic particles producing HF absorption, and are approximately colocated with MeV particle contamination on DMSP particle sensors. Diffuse regions of precipitation often appear to break up, especially on the poleward edge, into small irregular swirls and spots, which we have termed angels, distributed over wide regions and moving more or less in unison. These features, which evidence little or no L-shell control on their alignment, appear to be most prevalent during the recovery phase after an active period, although there appears to be a continuum of forms ranging from L-shell aligned diffuse bands to mixed diffuse and structured precipitation on to isolated small-scale structures. One possible explanation suggested by our observations is that the precipitation structure directly reflects structure in the cold plasma inside the plasmasphere being enhanced near the plasmapause. This can be tested in the future by searching for the VLF hiss which should accompany the optically observed precipitation. Due to the association of this type of precipitation with HF absorption, its presence has a pronounced but previously unrecognized impact on HF heating experiments in the near-subauroral region. An understanding of the dynamics of this natural particle population and instabilities in these regions is essential to efforts to alter these particle populations by artificial means. Finally, several substorm-related phenomena observed in association with the data presented in this report add to a consistent picture of the interrelation between ring current injection events and the outer radiation belt, namely the co-location of the inner SAPS boundary and the poleward boundary of the radiation belt, consistent with statistical studies of plasmapause and radiation belt boundary locations.

[45] **Acknowledgments.** We thank Fred Rich for help with DMSP data processing and discussion. This work was sponsored primarily by the Air Force Office of Scientific Research task 2311AS and by AFRL contract F19628-02-C-0087 with Boston College. HAARP is a Department of Defense project operated jointly by the U. S. Air Force and U. S. Navy.

[46] Wolfgang Baumjohann thanks Dag Lorentzen and Charles Deehr for their assistance in evaluating this paper.

References

Akasofu, S.-I. (1977), *Physics of Magnetospheric Substorms*, D. Reidel, Dordrecht, Netherlands.

Anger, C., M. Moshupi, D. Wallis, J. Murphree, L. Brace, and G. Shepherd (1978), Detached auroral arcs in the trough region, *J. Geophys. Res.*, *83*, 2683.

Brice, N. (2001), Differential drift of plasma clouds in the magnetosphere, *J. Atmos. Sol. Terr. Phys.*, *63*, 1275.

Burke, W., A. Rubin, D. Hardy, and E. Holeman (1995), Banded electron structures in the plasmasphere, *J. Geophys. Res.*, *100*, 7759.

Carpenter, D. L., M. A. Spasojevic, T. F. Bell, U. S. Inan, B. W. Reinisch, I. A. Galkin, R. F. Benson, J. L. Green, S. F. Fung, and S. A. Boardsen (2002), Small-scale field-aligned plasmaspheric density structures inferred from the Radio Plasma Imager on IMAGE, *J. Geophys. Res.*, *107*(A9), 1258, doi:10.1029/2001JA009199.

Chen, A., and R. Wolf (1972), Effect on the plasmasphere of a time-varying convection electric field, *Planet. Space Sci.*, *20*, 483.

Erickson, P. J., J. C. Foster, and J. M. Holt (2002), Inferred electric field variability in the polarization jet from Millstone Hill E region coherent scatter observations, *Radio Sci.*, *37*(2), 1027, doi:10.1029/2000RS002531.

Evans, D. S., and M. S. Greer (2000), Polar Orbiting Environmental Satellite Space Environment Monitor 2: Instrument description and archive data documentation, *Tech. Memo. OAR SEC-93*, NOAA, Boulder, Colo.

Feldstein, Y., and Y. Galperin (1985), The auroral luminosity structure in the high-latitude upper atmosphere—Its dynamics and relationship to the large-scale structure of the earth's magnetosphere, *Rev. Geophys.*, *23*, 217.

Foster, J., and W. Burke (2002), A new categorization for subauroral electric fields, *Eos Trans. AGU*, *83*, 393.

Goldstein, J., B. Sandel, P. Reiff, and M. Hairston (2003), Control of plasmaspheric dynamics by both convection and sub-auroral polarization stream, *Geophys. Res. Lett.*, *30*(24), 2243, doi:10.1029/2003GL018390.

Goldstein, J., S. Kanekal, D. Baker, and B. Sandel (2005a), Dynamic relationship between the outer radiation belt and the plasmapause during March–May 2001, *Geophys. Res. Lett.*, *32*, L15104, doi:10.1029/2005GL023431.

Goldstein, J., J. Burch, B. Sandel, S. Mende, P. C. son Brandt, and M. Hairston (2005b), Coupled response of the inner magnetosphere and ionosphere on 17 April 2002, *J. Geophys. Res.*, *110*, A03205, doi:10.1029/2004JA010712.

Greenwald, R. A., K. Oksavik, P. J. Erickson, F. D. Lind, J. M. Ruohoniemi, J. B. H. Baker, and J. W. Gjerloev (2006), Identification of the temperature gradient instability as the source of decameter-scale ionospheric irregularities on plasmapause field lines, *Geophys. Res. Lett.*, *33*, L18105, doi:10.1029/2006GL026581.

Hardy, D. A., L. K. Schmidt, M. S. Gussenhoven, F. J. Marshall, H. C. Yeh, T. L. Shumaker, A. Huber, and J. Pantazis (1984), Precipitating electron and ion detectors (SSJ/4) for block 5D/Flights 4–10 DMSP satellites: Calibration and data presentation, *Tech. Rep. AFGL-TR-84-0317*, Air Force Geophys. Lab., Hanscom Air Force Base, Mass.

Huang, C., S. Sazykin, R. Spiro, J. Goldstein, G. Crowley, and M. Ruohoniemi (2006), Storm-time penetration electric fields and their effects, *Eos Trans. AGU*, *87*, 131.

Hudson, M. K., and M. C. Kelley (1976), The temperature gradient instability at the equatorward edge of the ionospheric plasma trough, *J. Geophys. Res.*, *81*, 3913.

Inan, U., et al. (2004), Multi-hop whistler-mode ELF/VLF signals and triggered emissions excited by the HAARP heater, *Geophys. Res. Lett.*, *31*, L24805, doi:10.1029/2004GL021647.

Kadomtsev, B. (1965), *Plasma Turbulence*, Academic, New York.

Kubota, M., T. Nagatsuma, and Y. Murayama (2003), Evening co-rotating patches: A new type of aurora observed by high-sensitivity all-sky cameras in Alaska, *Geophys. Res. Lett.*, *30*(12), 1612, doi:10.1029/2002GL016652.

Li, X., D. Baker, T. O'Brien, L. Xie, and Q. Zong (2006), Correlation between the inner edge of outer radiation belt electrons and the innermost plasmapause location, *Geophys. Res. Lett.*, *33*, L14107, doi:10.1029/2006GL026294.

Liemohn, M., G. Khazanov, and J. Kozyra (1998), Banded electron structure formation in the inner magnetosphere, *Geophys. Res. Lett.*, *25*, 877.

Lin, C., H.-C. Yeh, B. Sandel, J. Goldstein, F. Rich, W. Burke, and J. Foster (2007), Magnetospheric convection near the drainage plume, *J. Geophys. Res.*, *112*, A05216, doi:10.1029/2006JA011819.

Mendillo, M., J. Baumgardner, and J. Providakes (1989), Ground-based imaging of detached arcs, ripples in the diffuse aurora, and patches of 6300-Å emission, *J. Geophys. Res.*, *94*, 5367.

Mishin, E., and W. Burke (2005), Stormtime coupling of the ring current, plasmasphere and topside ionosphere: Electromagnetic and plasma disturbances, *J. Geophys. Res.*, *110*, A07209, doi:10.1029/2005JA011021.

Mishin, E., J. Foster, A. Potekhin, F. Rich, K. Schlegel, K. Yumoto, V. Taran, J. Ruohoniemi, and R. Friedel (2002), Global ULF disturbances during a stormtime substorm on 25 September 1998, *J. Geophys. Res.*, *107*(A12), 1486, doi:10.1029/2002JA009302.

Moldwin, M., J. Howard, J. Sanny, J. Bocchicchio, H. Rassoul, and R. Anderson (2004), Plasmaspheric plumes: CRRES observations of enhanced density beyond the plasmapause, *J. Geophys. Res.*, *109*, A05202, doi:10.1029/2003JA010320.

Moshupi, M., C. Anger, J. Murphree, D. Wallis, J. Whitteker, and L. Brace (1979), Characteristics of trough region auroral patches and detached arcs observed by ISIS 2, *J. Geophys. Res.*, *84*, 1333.

Newell, P. (2003), Atmospheric physics: A new dawn for aurora, *Nature*, *424*, 734, doi:10.1038/424734a.

Ober, D., J. Horwitz, and D. Gallagher (1997), Formation of density troughs embedded in the outer plasmasphere by subauroral ion drift events, *J. Geophys. Res.*, *102*, 14,595.

Oksavik, K., R. A. Greenwald, J. M. Ruohoniemi, M. R. Hairston, L. J. Paxton, J. B. H. Baker, J. W. Gjerloev, and R. J. Barnes (2006), First observations of the temporal/spatial variation of the sub-auroral polarization stream from the SuperDARN Wallops HF radar, *Geophys. Res. Lett.*, *33*, L12104, doi:10.1029/2006GL026256.

Ono, T., T. Hirasawa, and C. Meng (1987), Proton auroras observed at the equatorward edge of the duskside auroral oval, *Geophys. Res. Lett.*, *14*, 660.

Pierrard, V., and J. Lemaire (2004), Development of shoulders and plumes in the frame of the interchange instability mechanism for plasmapause formation, *Geophys. Res. Lett.*, *31*, L05809, doi:10.1029/2003GL018919.

Rich, F. J., and M. Hairston (1994), Large-scale convection patterns observed by DMSP, *J. Geophys. Res.*, *99*, 3827.

Rosenberg, T. J., D. L. Detrick, D. Venkatesan, and G. van Bavel (1991), A comparative study of imaging and broad-beam riometer measurements: The effect of spatial structure on the frequency dependence of auroral absorption, *J. Geophys. Res.*, *96*, 17,793.

Stubbe, P., H. Kopka, and R. Dowden (1981), Generation of ELF and VLF waves by polar electrojet modulation: Experimental results, *J. Geophys. Res.*, *86*, 9073.

Toyoshima, S., H. Fukunishi, N. Yoshida, M. Kubota, and Y. Murayama (2003), Characteristics of the corotating aurora observed at Poker Flat, Extended Abstract, *Tohoku Geophys. J.*, *30*, 514.

Wallis, D. D., J. R. Burrows, M. C. Moshupi, C. D. Anger, and J. S. Murphree (1979), Observations of particles precipitating into detached arcs and patches equatorward of the auroral oval, *J. Geophys. Res.*, *84*, 1347.

Yizengaw, E., and M. Moldwin (2005), The altitude extension of the mid-latitude trough and its correlation with the plasmapause position, *Geophys. Res. Lett.*, *32*, L09105, doi:10.1029/2005GL022854.

Yizengaw, E., H. Wei, M. Moldwin, D. Galvan, L. Mandarake, A. Mannucci, and X. Pi (2005), The correlation between mid-latitude trough and the plasmapause, *Geophys. Res. Lett.*, *32*, L10102, doi:10.1029/2005GL022954.

Zhang, Y., L. J. Paxton, D. Morrison, B. Wolven, H. Kil, and S. Wing (2005), Nightside detached auroras due to precipitating protons/ions during intense magnetic storms, *J. Geophys. Res.*, *110*, A02206, doi:10.1029/2004JA010498.

E. Mishin, Institute for Scientific Research, Boston College, 402 St Clements Hall, 140 Commonwealth Ave., Chestnut Hill, MA 02467-3862, USA. (evgenii.mishin@hanscom.af.mil)

K. Oksavik, Johns Hopkins University Applied Physics Laboratory, 11100 Johns Hopkins Road, Laurel, MD 20723, USA. (kjellmar.oksavik@jhuapl.edu)

T. Pedersen, Space Vehicles Directorate, Air Force Research Laboratory, Hanscom AFB, MA 01731, USA. (todd.pedersen@hanscom.af.mil)